sciendo

Int. J. of Applied Mechanics and Engineering, 2019, vol.24, No.4, pp.125-139
DOI: 10.2478/ijame-2019-0053

THE IMPACT OF RADIATION EFFECT ON MHD STAGNATION-POINT FLOW OF A NANOFLUID OVER AN EXPONENTIALLY STRETCHING SHEET IN THE PRESENCE OF CHEMICAL REACTION

G. NARENDER* and G. SREEDHAR SARMA
CVR College of Engineering, Department of Humanities and Sciences
Hyderabad-501510, INDIA
E-mail: gnriimc@gmail.com; sarma.sreedhar@gmail.com

K. GOVARDHAN
GITAM University, Hyderabad-502329
Telangana State, INDIA
E-mail: govardhan_kmtm@yahoo.co.in

The present study is to investigate the effect of the chemical reaction parameter on stagnation point flow of magnetohydrodynamics field past an exponentially stretching sheet by considering a nanofluid. The problem is governed by governing coupled nonlinear partial differential equations with appropriate boundary conditions. The transformed non-dimensional and coupled governing ordinary differential equations are solved numerically using the fourth order Adams-Bashforth Moulton method. The effects of various dimensionless parameters on velocity, temperature and concentration fields are studied and then the results are presented in both tabular and graphical forms.

Key words: numerical solution, MHD, radiation effect, stagnation-point flow, chemical reaction, nanofluid.

1. Introduction

Nanofluids are important to study because of their heat and mass transfer properties. They enhance the thermal conductivity and convective properties over the properties of the base fluid. The study of heat and mass transfer with chemical reaction is of great practical importance to engineers and scientists because of its almost universal occurrence in many branches of science and engineering. Moreover, such fluids when compared with the conventional heat transfer fluids, have a much higher rate of thermal conduction and exhibit significant characteristics. Owing to their enhanced features, nanofluids have immense applications in automobile industries, medical arena, power plant cooling systems, nuclear engineering and a lot more. Moreover, several research studies have been performed by considering the different aspects of the flows past a stretching sheet.

Choi in [1] used the term nanofluid for the first time, which is the colloidal mixture of nanoparticles and base fluid. Most of the research has shown that metallic particles transfer more heat energy as compared to non-metallic particles. Buongiorno [2] presented a simple convective model to analyze transport in nanofluids and implied that energy transfer by dispersion of nanoparticles was negligible. In the boundary layer, there may be a decrease in viscosity, which will lead to heat transfer enhancement. An excellent assessment of nanofluid physics and developments was provided by Cheng [3]. Buongiorno and Hu [4] analyzed the convective heat transfer enhancement had been suggested to be due to the dispersion of the suspended nanoparticles, this effect was too small to explain the observed enhancement. It is often assumed

* To whom correspondence should be addressed

in the problems of boundary layer flow over a stretching surface that the velocity of the stretching surface is linearly proportional to the distance from the fixed origin. However, Gupta and Gupta [5] argued against the linearity condition. In the past few years, noted the stretching of plastic sheet may not necessarily be linear. For example, Emmanuel and Khan [6] considered MHD flow past an exponentially stretching sheet. Heat transfer in a viscoelastic boundary layer flow over a stretching sheet with non-uniform heat source and viscous dissipation was studied by Subhas and Siddheshwar [7]. The effect of thermal radiation on the flow was examined by Nadeem *et al*. [8]. Al-odat *et al*. [9] obtained the results on the effect of a magnetic field on an exponential temperature distribution on a stretching sheet. Chand and Jat [10] considered an unsteady stretching surface in a porous medium and explained the thermal radiation and viscous dissipation effects on a magnetohydrodynamic flow over it. Ishak [11] worked on the MHD boundary layer flow due to an exponentially stretching sheet with radiation effect. Flow through a porous medium bounded by a vertical surface in the presence of Hall current was explained by Sudhakar *et al.* [12]. Bidin and Nazar [13] numerically investigated the MHD boundary layer flow over an exponentially stretching sheet with thermal radiation.

The objective of this paper is to extend the work of Anwar *et al*. [14] by taking into account radiation effect on an MHD stagnation-point flow of a nanofluid over an exponentially stretching sheet in the presence of chemical reaction.

2. Mathematical formulation

A two-dimensional boundary layer flow of a viscous, Newtonian and incompressible nanofluid through a delete plate in a porous medium has been considered with focus on the heat and mass transfer. The geometry of the flow model is shown in Fig.1. The stretching velocity and free stream velocities are assumed to be of the forms $u_w(x) = ae^{\left(\frac{x}{l}\right)}$ and $u_\infty(x) = be^{\left(\frac{x}{l}\right)}$ where a and b are constants. The magnetic field of strength $B(x) = B_0 e^{\left(\frac{x}{2l}\right)}$ is applied perpendicular to the stretching sheet. The coordinate system is chosen in a manner that the $x-$axis is along the flow whereas the $y-$axis is perpendicular to the flow. Furthermore, the direction of the uniform magnetic field is chosen in such a manner that it is normal to the surface of the fluid flow. The effects of Brownian motion and thermophoresis have been elaborated. Moreover, the convective surface conditions have been taken into consideration.

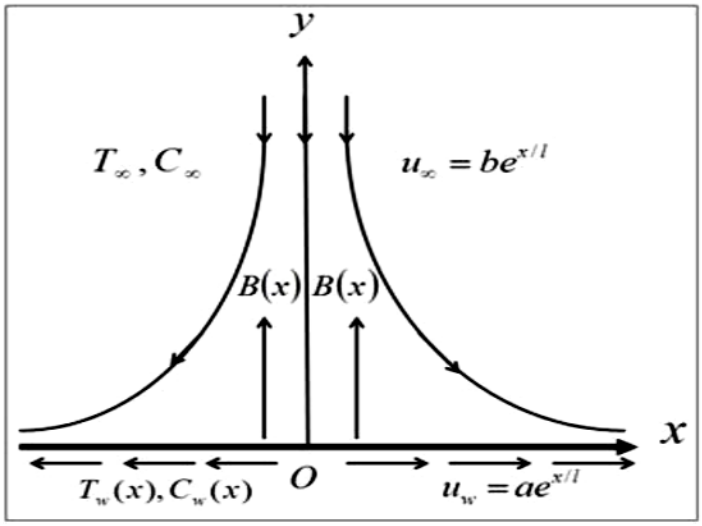

Fig.1. Physical model and coordinate system.

The flow is described by the equation of continuity, equation of momentum, the energy equation and concentration equation as

$$\frac{\partial u}{\partial x}+\frac{\partial v}{\partial y}=0, \tag{2.1}$$

$$\frac{\partial u}{\partial x}u+\frac{\partial u}{\partial y}v=-\frac{\sigma B_0^2}{\rho_f}\left(u-U_\infty\right)+\nu\left(\frac{\partial^2 u}{\partial x^2}+\frac{\partial^2 u}{\partial y^2}\right)+U_\infty\frac{\partial U_\infty}{\partial x}, \tag{2.2}$$

$$\begin{aligned}&\frac{\partial T}{\partial x}u+\frac{\partial T}{\partial y}v=-\frac{\nu}{\rho c_f}\left(\frac{\partial u}{\partial y}\right)^2+\alpha\left(\frac{\partial^2 T}{\partial x^2}+\frac{\partial^2 T}{\partial y^2}\right)-\frac{1}{\left(\rho c_p\right)_f}\frac{\partial q_r}{\partial y}+\\&+\tau\left\{D_B\left(\frac{\partial C}{\partial y}\frac{\partial T}{\partial y}+\frac{\partial C}{\partial x}\frac{\partial T}{\partial x}\right)+\frac{D_T}{T_\infty}\left[\left(\frac{\partial T}{\partial x}\right)^2+\left(\frac{\partial T}{\partial t}\right)^2\right]\right\},\end{aligned} \tag{2.3}$$

$$\frac{\partial C}{\partial x}u+\frac{\partial C}{\partial y}v=D_B\left(\frac{\partial^2 C}{\partial x^2}+\frac{\partial^2 C}{\partial y^2}\right)-\frac{D_T}{T_\infty}\left(\frac{\partial^2 T}{\partial x^2}+\frac{\partial^2 T}{\partial y^2}\right)-C_0\left(C-C_\infty\right). \tag{2.4}$$

In the above equations, μ is the kinematic viscosity, ρ_f is the density of the base fluid, σ is the electrical conductivity, $B(x)$ is the magnetic field, $\alpha=\dfrac{\xi}{(\rho c)_f}$ where ξ is the thermal conductivity and $(\rho c)_f$ is the heat capacitance of the base fluid, τ is the parameter defined by $\tau=\dfrac{(\rho c)_p}{(\rho c)_f}$, $(\rho c)_p$ is the effective heat capacity of a nanoparticle, D_B is the Brownian diffusion, q_r is the radiation flux.

The Rosseland approximation has been considered for radiation and the formula for the radiative heat flux q_r is stated below.

$$q_r=\frac{-4\sigma^*}{3k^*}\frac{\partial T^4}{\partial y}. \tag{2.5}$$

For smaller values of temperature contrast, the temperature difference T^4 might be expanded about T_∞ using Taylor series, as follows

$$T^4=T_\infty^4+\frac{4T_\infty^3}{1!}\left(T-T_\infty\right)+\frac{12T_\infty^2}{2!}\left(T-T_\infty\right)^2+\frac{24T_\infty^3}{3!}\left(T-T_\infty\right)^3+\ldots\ldots\ldots \tag{2.6}$$

omitting the terms having higher order, we get

$$T^4=4T_\infty^3T-3T_\infty^4. \tag{2.7}$$

Then

$$\Rightarrow \frac{\partial T^4}{\partial y} = 4T_\infty^3 \frac{\partial T}{\partial y}. \tag{2.8}$$

Using Eq.(2.8) in Eq.(2.5) and differentiating, we have the following form

$$\frac{\partial q_r}{\partial y} = -\frac{16\sigma^* T_\infty^3}{3k^*}\frac{\partial^2 T}{\partial y^2}. \tag{2.9}$$

Then Eq.(2.3) gets the following form

$$\begin{aligned}&\frac{\partial T}{\partial x}u + \frac{\partial T}{\partial y}v = -\frac{\nu}{\rho c_f}\left(\frac{\partial u}{\partial y}\right)^2 + \alpha\left(\frac{\partial^2 T}{\partial x^2} + \frac{\partial^2 T}{\partial y^2}\right) + \\ &+\tau\left\{D_B\left(\frac{\partial C}{\partial y}\frac{\partial T}{\partial y} + \frac{\partial C}{\partial x}\frac{\partial T}{\partial x}\right) + \frac{D_T}{T_\infty}\left[\left(\frac{\partial T}{\partial x}\right)^2 + \left(\frac{\partial T}{\partial y}\right)^2\right]\right\} + \frac{16\sigma^* T_\infty^3}{3\left(\rho c_f\right)k^*}\frac{\partial^2 T}{\partial y^2}.\end{aligned} \tag{2.10}$$

The corresponding boundary conditions at the boundary surface are

$$u = U_w(x) = ae^{\left(\frac{x}{2l}\right)}, \quad v = 0, \quad T = T_w(x), \quad C = C_w(x) \quad \text{at} \quad y = 0, \tag{2.11a}$$

$$u \to U_\infty(x) = be^{\left(\frac{x}{2l}\right)}, \quad v = 0, \quad T \to T_\infty, \quad C \to C_\infty \quad \text{as} \quad y \to \infty. \tag{2.11b}$$

The prescribed temperature and the concentration on the surface of the sheet are $T_w(x) = T_\infty + T_0 e^{\left(\frac{x}{2l}\right)}, C_w(x) = C_\infty + C_0 e^{\left(\frac{x}{2l}\right)}$. Here T_0, C_0 are the reference temperature and concentration, respectively.

Let ψ be the stream function satisfying the continuity equation in the following sense

$$u = \frac{\partial \psi}{\partial y}, \quad v = -\frac{\partial \psi}{\partial x}. \tag{2.12}$$

For the conversion of the mathematical model (2.1) - (2.4) into the dimensionless form, the following similarity transformation has been introduced

$$\eta = y\sqrt{\frac{a}{2\nu l}}e^{\left(\frac{x}{2l}\right)}, \quad \psi = \sqrt{2a\nu a}e^{\left(\frac{x}{2l}\right)}f(\eta), \quad \theta(\eta) = \frac{T - T_\infty}{T_f - T_\infty}, \quad \phi(\eta) = \frac{C - C_\infty}{C_w - C_\infty}. \tag{2.13}$$

The final dimensionless form of the governing model, is

$$f''' + ff'' - 2\left(f'\right)^2 + 2A^2 - \left(f' - A\right) = 0, \tag{2.14}$$

$$\left(1+\frac{4}{3}R\right)\theta''+\Pr\left(f\theta'-f'\theta+Nb\phi'\theta'+Nt\left(\theta^{1}\right)^{2}\right)=0, \tag{2.15}$$

$$\phi''+\mathrm{Le}\left(f\phi'-f'\phi\right)+\frac{Nt}{Nb}\theta''-\mathrm{Le}\chi\phi=0. \tag{2.16}$$

The transformed boundary conditions are stated below

$$\begin{aligned} &f(0)=0,\quad f'(0)=1,\quad \theta(0)=1,\quad \phi(0)=1 \quad \text{at} \quad y=0,\\ &f'(\infty)\to A,\quad \theta(\infty)\to 0,\quad \phi(\infty)\to 0 \quad \text{as} \quad \eta\to\infty. \end{aligned} \tag{2.17}$$

.

Different parameters used in the above equations have the following formulations:

$R=\dfrac{4T_\infty\sigma^*}{k^*k}$, is the radiation parameter,

$\Pr=\dfrac{\nu}{\alpha}$ is the Prandtl number,

$\mathrm{Le}=\dfrac{\nu}{D_B}$, is the Lewis number,

$M=\dfrac{2l\sigma B_0^2}{\rho_f a}$, is the magnetic parameter,

$A=\dfrac{b}{a}$ is the velocity ratio parameter,

$Nb=\dfrac{\tau D_B\left(C_f-C_\infty\right)}{\nu}$, is the Browian motion parameter,

$Nt=\dfrac{\tau D_T\left(T_f-T_\infty\right)}{\nu T_\infty}$, is the thermophoresis parameter and

$\chi=\dfrac{C_0}{a}$ is the reaction rate parameter.

The major interest of the study is to calculate the skin-friction coefficient C_f, the reduced Nusselt number $-\theta'(0)$ and the reduced Sherwood number $-\phi'(0)$ which are given as follows

$$C_f\sqrt{\frac{2l}{x}\mathrm{Re}_x} = f''(0), \quad \frac{\mathrm{Nu}}{\sqrt{\frac{2l}{x}\mathrm{Re}_x}} = -\left[1+\frac{4}{3}R\right]\theta'(0), \quad \frac{\mathrm{Sh}}{\sqrt{\frac{2l}{x}\mathrm{Re}_x}} - \phi'(0) \tag{2.18}$$

where, $\mathrm{Re} = \frac{xU_w}{\nu}$ elucidates the local Reynolds number and $\nu = \frac{\mu}{\rho}$ the kinematic viscosity.

3. Numerical technique

The numerical solution of the mathematical model in the form of non-linear differential Eqs (2.14)-(2.15) along with the boundary conditions (2.17) was reported by Imran Anwar *et al*. [14]. They opted for the Keller-box method for the numerical solution of the above model. In the present section, the shooting technique has been proposed to reproduce the same solution. The Adams-Bashforth Moulton method of order four and the Newton's technique for solving the non-linear algebraic equations are the main components of the shooting technique.

To have a system of first order ODEs, use the notations

$$f = y_1, \quad f' = y_2, \quad f'' = y_3, \quad \theta = y_4, \quad \theta' = y_5, \quad \phi = y_6, \quad \phi' = y_7\,. \tag{3.1}$$

By using notations (24), we have the following IVP

$$\begin{aligned}
y_1' &= y_2, & y_1(0) &= 0,\\
y_2' &= y_3, & y_2(0) &= 1,\\
y_3' &= \left[-2y_2^2 - M(A-y_2) - y_1y_3\right], & y_3(0) &= r,\\
y_4' &= y_5, & y_4(0) &= 1,\\
y_5' &= -\frac{\mathrm{Pr}}{\left(1+\frac{4}{3}R\right)}\left[y_1y_5 - y_2y_4 + Nby_7y_5 + Nty_5^2\right], & y_5(0)) &= s,\\
y_6' &= y_7, & y_6(0) &= 1,\\
y_7' &= -\mathrm{Le}y_1y_7 - \mathrm{Le}y_2y_6 - \frac{Nt}{Nb}y_5' + \mathrm{Le}\chi y_6, & y_7(0) &= t.
\end{aligned} \tag{3.2}$$

where r, s and t are the initial guesses.

For the computational purpose, the unbounded domain $[0,\infty)$ has been replaced by a bounded domain $[0,\eta_\infty]$, where η_∞ is some suitable finite real number. It is chosen in such a way that the solutions

of the problem start looking settled for $\eta > \eta_\infty$. In Eqs (3.2), the missing initial conditions r, s and t are to be chosen such that

$$y_2(\eta_\infty, r, s, t) - A = 0, \quad y_4(\eta_\infty, r, s, t) = 0, \quad y_6(\eta_\infty, r, s, t) = 0. \tag{3.3}$$

To start the iterative process, choose $r = r_0, s = s_0$ and $t = t_0$. The initial guess is updated by the Newton's method until a solution of the problem which approximately meets the given boundary conditions at the right end of the domain. Next, the IVP in the first order ODEs given in Eq.(3.2) is solved by the Adams-Bash forth Moulton method.

The convergence criteria are chosen to be successive value agree up to 3 significant digits. The choice of $\eta_{\max} = 10$ was more than enough for end condition.

4. Result and discussion

Physically realistic numerical values were assigned to the pertinent parameters in the system in order to gain an insight into the flow structure with respect to the velocity, temperature, skin friction and Nusselt number. The results have been depicted graphically and their detailed physical explanation also given. Table 1 below shows the Nusselt number $-\theta'(0)$ values for different values of the Prandtl number, Hartmann number and reaction rate parameter while the rest of the parameters are set to be zero where $Nt = Nb = A = \mathrm{Le} = 0$. The table shows the comparison between the results and those of [11, 13 and 14] and it shown that the results are in agreement.

Table 1. Comparison of the reduced Nusselt number $-\theta'(0)$ when $Nt = Nb = A = \mathrm{Le} = 0$.

Pr	M	R	Bidin and Nazar [13]	Ishak [11]	Imran Anwar *et al.* [14]	Present results
			$-\theta'(0)$			
1	*0*	*0*	*0.9548*	*0.9548*	*0.9548*	*0.9547822*
2	*0*	*0*	*1.4714*	*1.4714*	*1.4714*	*1.4714600*
3	*0*	*0*	*1.8691*	*1.8691*	*1.8691*	*1.8690730*
1	*0*	*1.0*	*0.5315*	*0.5312*	*0.5312*	*0.5317377*
1	*1.0*	*0*	-	*0.8611*	*0.8611*	*0.8610874*
1	*1.0*	*1.0*	-	*0.4505*	*0.4505*	*0.4513935*

Table 2 below shows the values of the local Nusselt number $-\theta'(0)$ and the local Sherwood number $-\phi'(0)$ when different values of all parameters involved are considered. It is observed from this table that $-\theta'(0)$ decreases with the increasing values of $Nb, \mathrm{Le}, R,$ and A. Whereas for increasing values of Pr, Nt, Nb and χ is increasing. However, it is found that $-\phi'(0)$ decreases for the increasing value of R whereas it increases for increasing values of $Nt, Nb, \mathrm{Pr}, \mathrm{Le}, M, A,$ and χ. Here, it is noted that for the increasing values of M, the local Nusselt number $-\theta'(0)$ and the local Sherwood number $-\phi'(0)$ show a quite opposite effect in both cases of $A < 1$ and $A > 1$.

Figure 2 shows how the magnetic parameter affects the velocity profiles $f'(\eta)$ when $A<1$, $A=1$ and $A>1$. It has been observed that $f'(\eta)$ decreases with an increase in the values of M for the case of $A<1$. The velocity reduces when the magnetic parameter increases in the case $A<1$. When the velocity of the stretching sheet is equal to the free stream velocity, there is no boundary layer thickness of nanofluid near the sheet $A=1$.

Table 2. Values of the local Nusselt number $-\theta'(0)$ and the local Sherwood number $-\phi'(0)$.

Nb	*Nt*	Pr	Le	*M*	*A*	*R*	χ	$-\theta'(0)$	$-\phi'(0)$	$-f'(0)$
0.1	*0.1*	*1*	*10*	*0.1*	*0.1*	*0.1*	*0.2*	*0 .5374883*	*3.4259970*	*1.2856510*
0.5	*0.1*	*1*	*10*	*0.1*	*0.1*	*0.1*	*0.2*	*0.4683891*	*3.5519440*	*1.2856510*
0.1	*0.5*	*1*	*10*	*0.1*	*0.1*	*0.1*	*0.2*	*0.5083771*	*2.9029440*	*1.2856510*
0.1	*0.1*	*10*	*10*	*0.1*	*0.1*	*0.1*	*0.2*	*1.6193550*	*2.9614960*	*1.2856510*
0.1	*0.1*	*1*	*25*	*0.1*	*0.1*	*0.1*	*0.2*	*0 .5358281*	*5.6791770*	*1.2856510*
0.1	*0.1*	*1*	*10*	*2.5*	*0.1*	*0.1*	*0.2*	*0 .4688037*	*3.3257190*	*1.8976840*
0.1	*0.1*	*1*	*10*	*2.5*	*1.1*	*0.1*	*0.2*	*0.8037469*	*3.6890500*	*-0 .2702405*
0.1	*0.1*	*1*	*10*	*0.1*	*0.9*	*0.1*	*0.2*	*0 .7565519*	*3.6181150*	*0 .2083470*
0.1	*0.1*	*1*	*10*	*0.1*	*1.1*	*0.1*	*0.2*	*0.7540233*	*3.6805980*	*-0.2216342*
0.1	*0.1*	*1*	*10*	*0.1*	*2.0*	*0.1*	*0.2*	*0.7221949*	*3.975730*	*-2.7517690*
0.1	*0.1*	*1*	*10*	*0.1*	*0.1*	*3.0*	*0.2*	*0.2762322*	*3.5029530*	*1.2881670*
0.1	*0.1*	*1*	*10*	*0.1*	*0.1*	*0.1*	*-1.0*	*0.7615607*	*0.8892360*	*1.2881670*
0.1	*0.1*	*1*	*10*	*0.1*	*0.1*	*0.1*	*1.0*	*0.7819918*	*4.3453950*	*1.2881670*
0.1	*0.1*	*1*	*10*	*0.1*	*0.1*	*0.1*	*5.0*	*0.8309667*	*7.6726790*	*1.2881670*

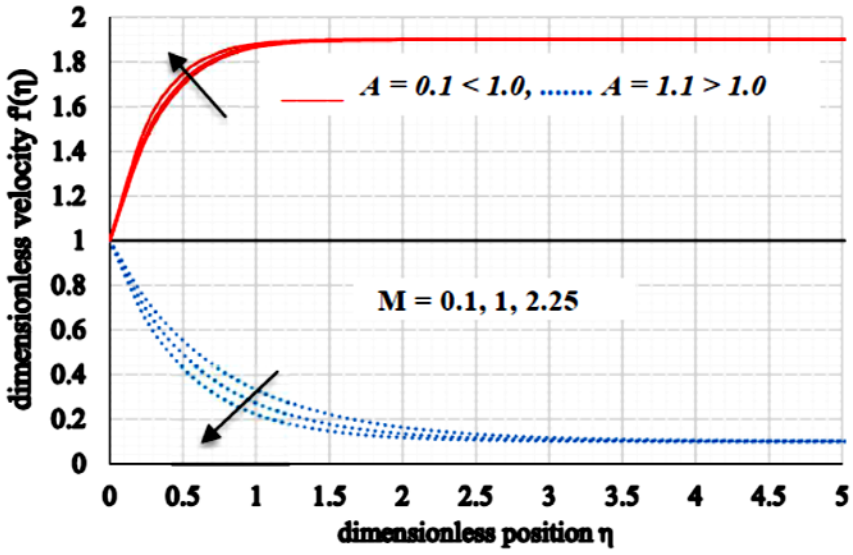

Fig.2. Velocity profiles vs M when $Nt=Nb=0.1$, $\Pr=\mathrm{Le}=2.0$, $R=1.0$, $\chi=0.1$.

Figure 3 illustrates the effect of the Brownian motion on the profile of temperature. So, distribution of the nanoparticle can be adjusted by adjusting the Brownian motion parameter.

Figure 4 displays the effect of the thermophoresis parameter Nt on the temperature profile. It is observed that the temperature increases with increasing the thermophoresis parameter. The temperature gradient generates thermophoresis force which creates a fast flow away from this surface. In this way more heated fluid is moved away from the surface and consequently, the temperature increases when Nt increases. It shows particularly that the effect of increasing the velocity ratio parameter A leads to a decrease in the temperature in the nanofluid.

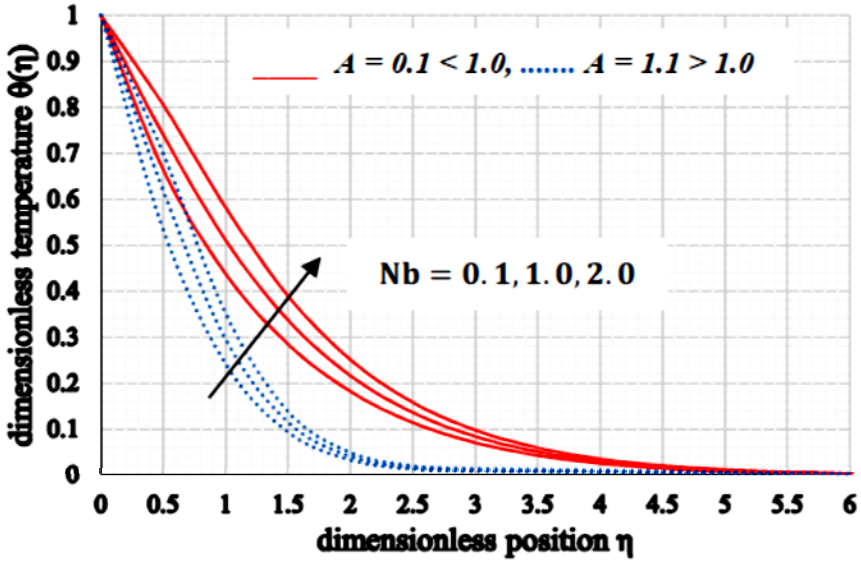

Fig.3. Temperature profiles vs Nb when $Nt = M = 0.1, \Pr = \mathrm{Le} = 2.0, R = 1.0, \chi = 0.1$.

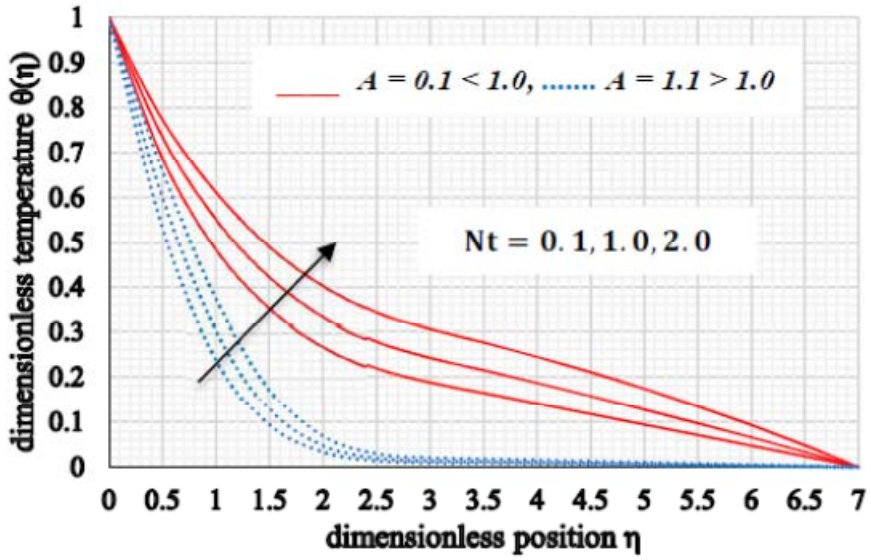

Fig.4. Temperature profiles vs Nt when $Nb = M = 0.1, \Pr = \mathrm{Le} = 2.0, R = 1.0, \chi = 0.1$.

Figure 5 is designed to see the influence of the thermal radiation R on the temperature $\theta(\eta)$. It is noticed that the temperature $\theta(\eta)$ enhances due to an increase in the radiation parameter. It is because of the

fact that for larger R the mean absorption coefficient k^* decreases which enhances the divergence of the radiative heat flux. Hence, the rate of the radiative heat transfer to the fluid will rise and consequently the fluid temperature increases.

Figure 6 reveals the influence of Pr on the dimensionless temperature profile. As expected, increasing Pr leads to a reduction in the dimensionless temperature. Based on the definition of Pr (the ratio of momentum diffusivity to thermal diffusivity), for large Pr heat will diffuse more rapidly than the momentum. Consequently, the thickness of thermal boundary layer reduces as Pr increases. It is also noticed that higher values of Pr reduce the temperature more drastically.

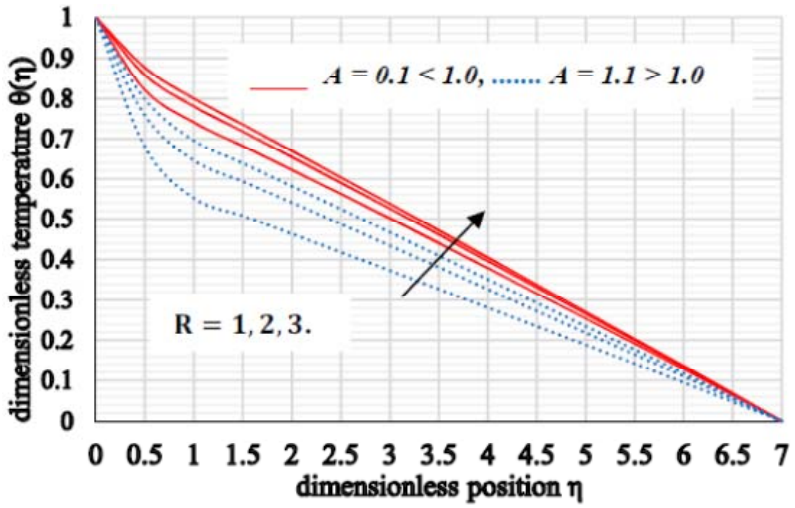

Fig.5. Temperature profiles vs R when $Nt = Nb = M = 0.1$, $\mathrm{Pr} = \mathrm{Le} = 2.0$, $R = 1.0$, $\chi = 0.1$.

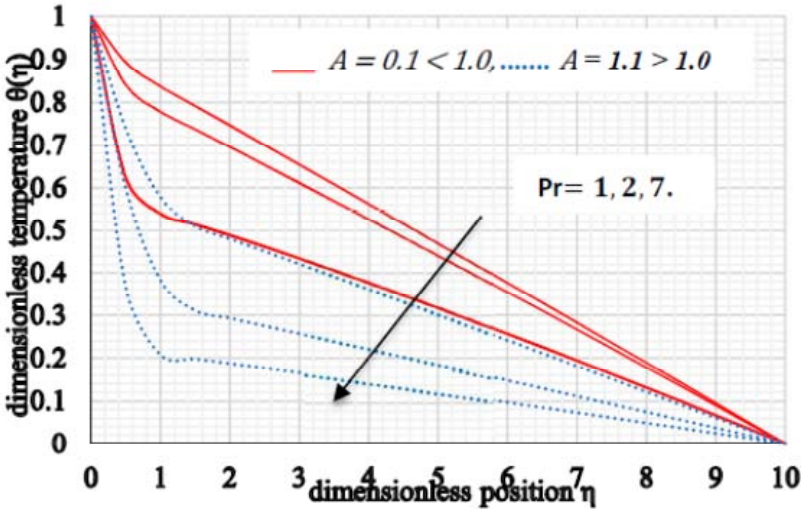

Fig.6. Temperature profiles vs Pr when $Nt = Nb = M = 0.1$, $\mathrm{Le} = 2.0$, $R = 1.0$, $\chi = 0.1$.

Figure 7 shows that $\theta(\eta)$ increases with increasing values of M when $A < 1$ while it decreases in the case of $A > 1$. It is noticed that the thermal boundary layer thickness is not much influenced by larger values of M when $A > 1$.

Figure 8 reveals the variation of concentration in response to a change in the Brownian motion parameter Nb. As the values of the Brownian motion parameter increase, the concentration boundary layer thickness is decreasing.

Figure 9 shows the variation of radiation on the concentration profile. The influence of the radiation parameter on concentration is not this much significant. As the values of the radiation parameter R increase, the concentration boundary layer thickness is not changing much. It can be observed from Tab.2 that as the radiation parameter R increases, the mass transfer rate is almost constant.

Figure 10. As the Lewis number increases the concentration graph decreases and the concentration boundary layer thickness decreases. This is probably due to the fact that the mass transfer rate increases as the Lewis number increases. Moreover, concentration at the surface of a sheet decreases as the values of Le increase.

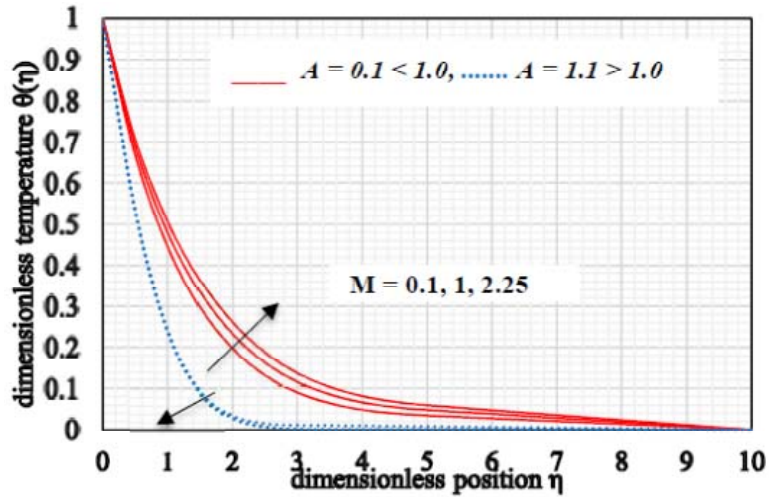

Fig.7. Temperature profiles vs M when $Nt = Nb = 0.1, \Pr = Le = 2.0, R = 1.0, \chi = 0.1$.

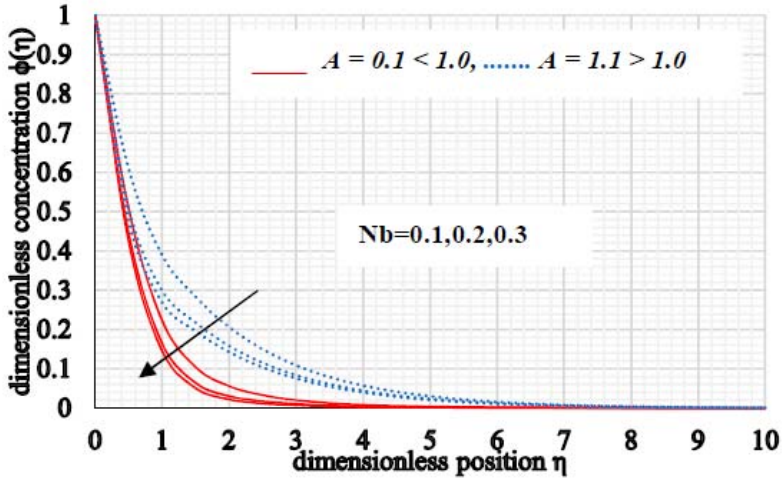

Fig.8. Concentration profiles vs Nb when $Nt = M = 0.1, \Pr = \mathrm{Le} = 2.0, R = 1.0, \chi = 0.1$.

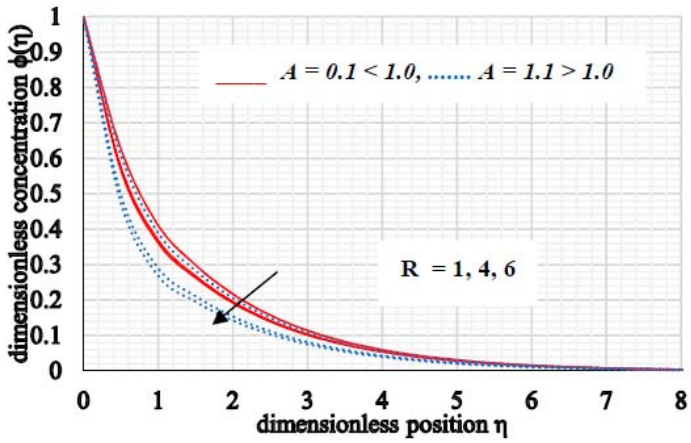

Fig.9. Concentration profiles vs R when $Nt = Nb = M = 0.1, \Pr = Le = 2.0, \chi = 0.1$.

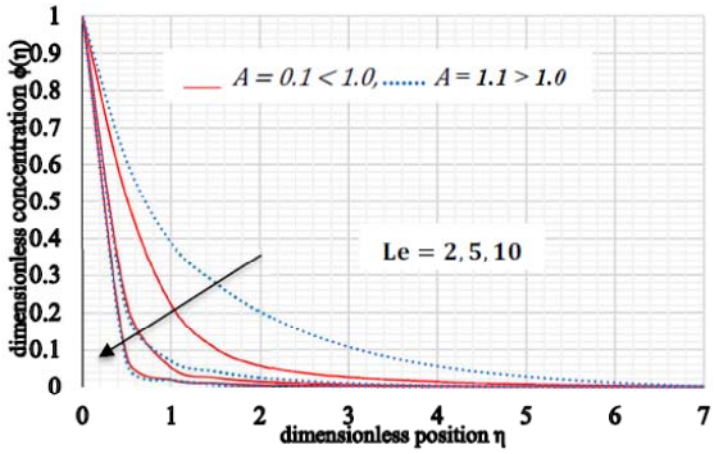

Fig.10. Concentration profiles vs Le when $Nt = Nb = M = 0.1$, $\Pr = 2.0$, $R = 0.1$, $\chi = 0.1$.

Figure 11 shows the concentration graph in response to a change in the thermophoresis parameter Nt. The influence of the thermophoresis parameter on the concentration profile graph is monotonic, i.e. as the values of Nt increase, the concentration boundary layer thickness is also increasing.

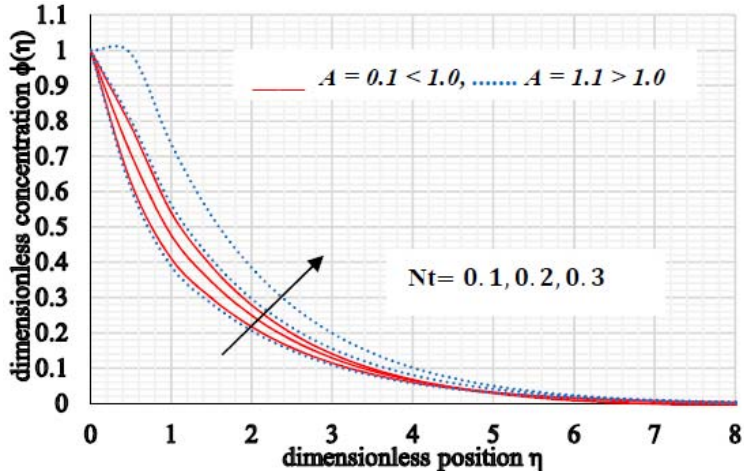

Fig.11. Concentration profiles vs Nt when $Nb = M = 0.1, \Pr = Le = 2.0, R = 1.0, \chi = 0.1$.

Figure 12. It is observed that the concentration profile diminishes with an increase in the chemical reaction. Nanoparticle concentration and layer thickness shrinkage is also noticed with the destructive chemical reaction.

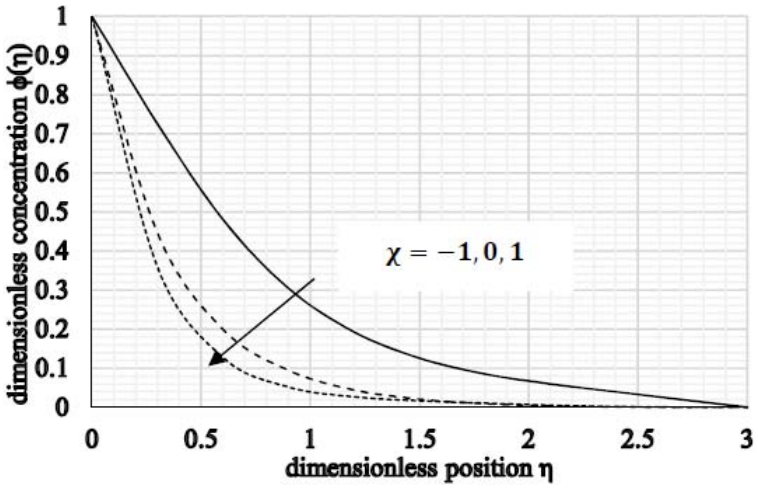

Fig.12. Concentration profiles vs χ when $Nb = M = 0.1$, $\mathrm{Pr} = \mathrm{Le} = 2.0$, $R = 1.0$, $A = 0.1$.

5. Conclusions

Some of the important findings of this observations are given below:

- The velocity bounded layer thickness shows an opposite behavior $A > 1$ and $A < 1$.
- For $A = 1$ there exists no boundary layer due to the fact that the fluid and sheet move at the same velocity.
- For large values of the chemical reaction parameter χ shows decreasing behavior.
- The concentration profile decreases an increase in chemical reaction parameter χ and Prandtl number.
- Increasing the Prandtl number decelerates the flow and strongly depresses temperature throughout the boundary layer regime, while the opposite behavior is seen in the case of enhancing the values of the Brownian motion parameter, thermophoresis parameter and radiation parameter.
- We noticed that concentration is decreased by increasing the Brownian motion, Lewis number.

Nomenclature

A – velocity ratio parameter
a,b,l – constants
B – magnetic field strength $(A.m^{-1})$
c_f – heat capacity of the fluid
c_p – effective heat capacity $(J.kg^{-1}K^{-1})$
D_B – Brownian diffusion coefficient
D_T – thermophoretic diffusion coefficient
k_0 – chemical reaction coefficient (s^{-1})
Le – Lewis number
M – magnetic parameter
Nb – Brownian motion parameter
Nr – radiation parameter

Nt – thermophoresis parameter
Nu – Nusselt number
Nur – reduced Nusselt number
Pr – Prandtl number
p – pressure
q_m – wall mass flux
q_w – wall heat flux
Re_x – local Reynolds number
Shr – reduced Sherwood number
Sh_x – local Sherwood number
T – fluid temperature
T_w – temperature at the stretching sheet
T_∞ – ambient temperature
u, v – velocity components along the x and y axis
u_w – velocity of the stretching surface
x, y – Cartesian coordinates (x axis is aligned along the stretching surface and y axis is perpendicular to it)
α – thermal diffusivity
β – dimensionless nanoparticle volume fraction
η – similarity variable
θ – dimensionless temperature
ξ – thermal conductivity $(W.m^{-1}.K^{-1})$.
ρ_f – density of fluid
ρ_p – mass density
σ – fluid electrical conductivity
τ – parameter defined by the ratio between the effective heat capacity of the nanoparticle material and heat capacity of the fluid. $\tau = (\rho c)_p / (\rho c)_f$
χ – chemical reaction parameter

References

[1] Choi S.U.S. (1995): *Enhancing thermal conductivity of fluids with nanoparticles*. – In: Siginer, D.A. and Wang, H.P., Eds. Developments and Applications of Non-Newtonian Flows, ASME, New York, pp.99-105.

[2] Buongiorno J. (2006): *Convective transport in nanofluids*. – ASME Journal of Heat Transfer, vol.128, pp.240-250.

[3] Cheng L. (2008): *Nanofluid two phase flow and thermal physics: a new research frontier of nanotechnology and its challenges*. – Journal of Nanoscience and Nanotechnology, vol.8, pp.3315-3332.

[4] Hu W. and Buongiorno J. (2005): *Nanofluid coolants for advanced nuclear power plants*. – Proceedings of ICAPP'05, Seoul, pp.15-19.

[5] Gupta P.S. and Gupta A.S. (1997): *Heat and mass transfer on a stretching sheet with suction or blowing.* – The Canadian Journal of Chemical Engineering, vol.55, pp.744-746.

[6] Emmanuel S. and Khan S.K. (2006): *On heat and mass transfer in a viscoelastic boundary layer flow over an exponentially stretching sheet.* – International Journal of Thermal Sciences, vol.45, pp.819-828.

[7] Subhas Abel M. and Siddheshwar P.G. (2007): *Heat transfer in a viscoelastic boundary layer flow over a stretching sheet with viscous dissipation and non-uniform heat source*. – International Journal of Heat and Mass Transfer, vol.50, pp.960-966.

[8] Nadeem S., Zaheer S. and Fang T.G. (2011): *Effects of thermal radiation on the boundary layer flow of a Jeffrey fluid over an exponentially stretching surface*. – Numerical Algorithms, vol.57, pp.187-205.

[9] Al-odat M.Q., Damseh R.A. and Al-azab T.A. (2006): *Thermal boundary layer on an exponentially stretching continuous surface in the presence of magnetic field effect*. – International Journal of Applied Mechanics and Engineering, vol.11, pp.289-299.

[10] Chand G. and Jat R.N. (2014): *Flow and heat transfer over an unsteady stretching surface in a porous medium.* – Thermal Energy and Power Engineering, vol.3, pp.266-272.

[11] Ishak (2011): *MHD boundary layer flow due to an exponentially stretching sheet with radiation effect*. – Sains Malays., vol.40, pp.391-395.

[12] Sudhakar K., Srinivas Raju R. and Rangamma M. (2013): *Hall effect on an unsteady MHD flow past along a porous flat plate with thermal diffusion, diffusion thermo and chemical reaction.* – Journal of Physical and Mathematical Sciences, vol.4, pp.370-395.

[13] Bidin B. and Nazar R. (2009): *Numerical solution of the boundary layer flow over an exponentially stretching sheet with thermal radiation.* – Eur. J. Sci. Res., vol.33, pp.710-7.

[14] Anwar I., Shafie S. and Salleh M.Z. (2014): *Radiation effect on MHD stagnation-point nanofluid over an exponentially stretching sheet*. – Walailak J. Sci. and Tech., vol.11, No.7, pp.569-591.

Received: July 20, 2018

Revised: October 16, 2019